LETTERS
PUBLISHED ONLINE: 24 JANUARY 2010 | DOI: 10.1038/NMAT2625
nature materials

Portrait of the potential barrier at metal–organic nanocontacts

Lucia Vitali[1]*, Giacomo Levita[1,2], Robin Ohmann[1], Alessio Comisso[3], Alessandro De Vita[3] and Klaus Kern[1,4]

Electron transport through metal–molecule contacts greatly affects the operation and performance of electronic devices based on organic semiconductors[1–4] and is at the heart of molecular electronics exploiting single-molecule junctions[5–8]. Much of our understanding of the charge injection and extraction processes in these systems relies on our knowledge of the potential barrier at the contact. Despite significant experimental and theoretical advances a clear rationale of the contact barrier at the single-molecule level is still missing. Here, we use scanning tunnelling microscopy to probe directly the nanocontact between a single molecule and a metal electrode in unprecedented detail. Our experiments show a significant variation on the submolecular scale. The local barrier modulation across an isolated 4-[*trans*-2-(pyrid-4-yl-vinyl)] benzoic acid molecule bound to a copper(111) electrode exceeds 1 eV. The giant modulation reflects the interaction between specific molecular groups and the metal and illustrates the critical processes determining the interface potential. Guided by our results, we introduce a new scheme to locally manipulate the potential barrier of the molecular nanocontacts with atomic precision.

The electronic structure at the interface between a bulk metal and an organic semiconductor thin film has been extensively studied[9–11] and is commonly described in the framework of a band alignment model at the interface. In the single-molecule case, however, this model faces its limits. Chemical bonding between an organic molecule and a metal surface can result in significant charge transfer and rearrangement, which depend critically on the local atomic geometry[5,12]. In this situation of a strongly hybridized electronic system, a good indicator of the physical and chemical processes determining the molecule–metal contact is the work function, which for metal substrates is defined as the energy difference between the vacuum level far above the surface and the Fermi level (see also Fig. 1a; ref. 13).

The formation of induced dipoles at the interface owing to the bonding of molecules can substantially modify the work function, which thereby provides valuable information on the degree of charge reorganization at the interface[13–15]. Photoemission experiments, often used to determine the averaged, coverage-dependent work function of a surface[11,16,17], have generated considerable progress in understanding the formation of the interface built-in potential. However, these experiments cannot provide any information at the molecular length scale. Lateral resolution can be achieved by photoemission of adsorbed Xe, scanning tunnelling or Kelvin probe measurements[13,18–20]. These experiments have revealed local modifications of the work function but could not probe a single-molecule contact with submolecular resolution. A quantity closely related to the work function is the local potential-energy barrier experienced by tunnelling electrons during scanning tunnelling microscopy (STM) measurements. This barrier can be used to measure a 'position-dependent work function'[13,18,21].

Here we measure for the first time the local spatial variation of the work function of a single-molecule–metal contact. Our STM experiments reveal a variation of more than 1 eV across an isolated functional organic molecule (4-[*trans*-2-(pyrid-4-yl-vinyl)] benzoic acid, hereafter PVBA; see Fig. 1b) bound to a Cu(111) surface. The chemical structure of this molecule, which shows two different functional (hetero-) aromatic groups, prompts characteristic interactions with the surface. On a submolecular scale these involve both π conjugation and chemical bonding to the supporting metal. Indeed, the STM topographic resolution and the spectroscopic capability provide a unique way to unravel the formation of the potential barrier. The direct comparison with theoretical predictions for the charge distribution at the interface facilitates a description of the effects of molecular bonding, charge transfer and surface-induced molecular dipoles on the potential-barrier profile.

The topographic image of a single isolated PVBA molecule adsorbed on Cu(111) is shown in Fig. 1c. Two white lobes and one major depression area can be recognized. The latter, which is associated with the oxygen-terminated molecular side (see also Supplementary Information), enables the assignment of the molecular orientation. The local potential barrier is obtained by fitting the tunnelling current recorded while varying the tip–sample distance (z). These two are related through $I \propto \exp(-2\sqrt{2m\Phi}/\hbar \times z)$, where m is the electron mass and Φ is the averaged work function $\Phi = (\Phi_T + \Phi_S)/2$ of tip and sample. The averaged work function can be extracted from the measurements as the slope of the logarithmic current plot as a function of z, for all lateral (x, y) tip positions. The potential barrier mapped across the nanocontact is reported in Fig. 1d, revealing a characteristic spatial dependence. Knowing the molecular structure and its adsorption orientation, this spatial dependence can be correlated with specific molecular groups. A potential-barrier increase is seen on the molecule, reflecting the shape of its (hetero-) aromatic backbone, whereas a reduction is observed in a rim region surrounding the molecule and is strongest near the oxygen termination. The relative variation of the work function with respect to the clean substrate measured along the molecular axis is reported in Fig. 1e. This has been calculated as $\Delta\Phi = 2(\Phi_{mol} - \Phi_{Cu})$, where Φ_{mol} and Φ_{Cu} are the barriers measured on the molecule and on the

[1]Max-Planck-Institut für Festkörperforschung, Heisenbergstr. 1, D-70569 Stuttgart, Germany, [2]INFM-DEMOCRITOS National Simulation Center and Center of Excellence for Nanostructured Materials (CENMAT), University of Trieste, via Valerio 6a, 34127 Trieste, Italy, [3]Physics Department, King's College London, Strand, London WC2R 2LS, UK, [4]Institut de Physique de la Matière Condensée, Ecole Polytechnique Fédérale de Lausanne (EPFL), CH-1015 Lausanne, Switzerland. *e-mail: lucia_vitali@ehu.es.

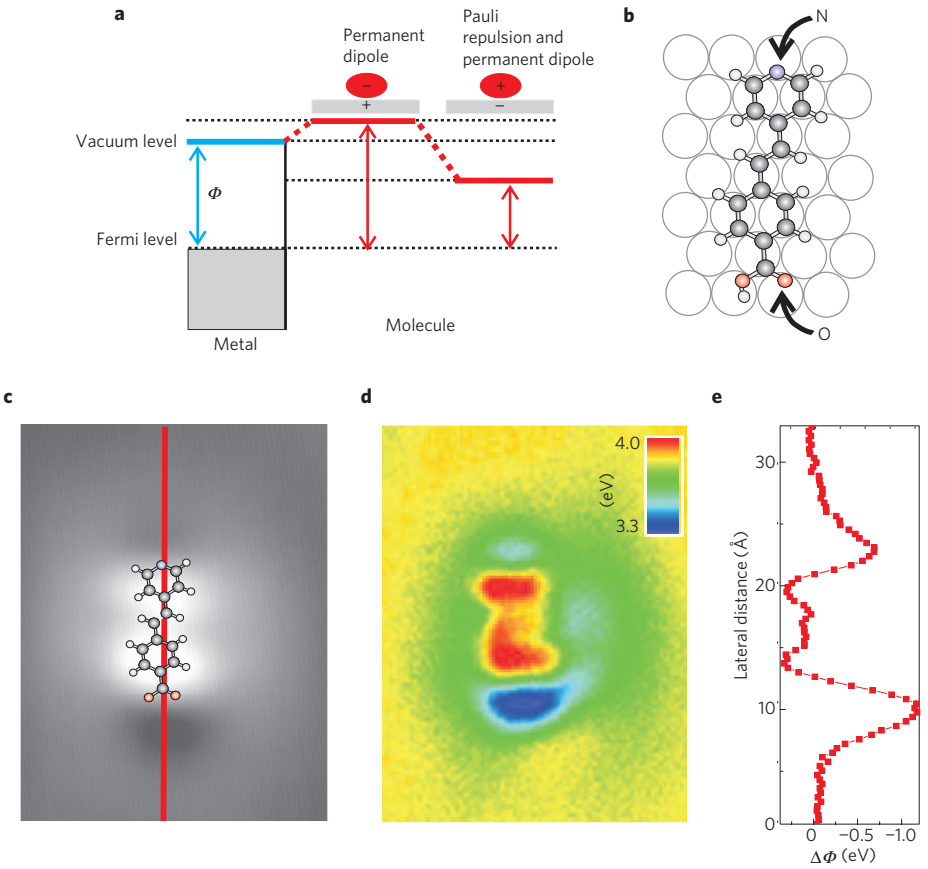

Figure 1 | Potential barrier across the plane of a molecule–metal nanocontact. a, Sketch of the work function on a clean metal (blue arrow) and at a conducting metal/organic interface (red arrow). The potential barrier is modified by two mechanisms: the formation of local dipoles and Pauli repulsion. The first is associated with chemisorption. If negative charge accumulates above (below) the surface, this opposes (favours) the withdrawal of an electron from the surface and results in an increase (decrease) of the local work function of the system. In the case of weak metal–organic coupling, Pauli repulsion between the electrons of the molecule and those of the metal surface is effective. This limits the spilling out of electrons into the vacuum region, and the electron density above (below) the metal surface moderately decreases (increases). **b**, Sketch of the neutral PVBA molecule. **c**, STM image of a deprotonated PVBA molecule adsorbed on Cu(111) measured in constant-current mode (image size, 33×25 Å^2; tunnelling conditions, -0.1 V; 0.5 nA). **d**, Simultaneously acquired map of the potential barrier across the molecular plane averaged between tip and sample. **e**, Work-function variation $\Delta\Phi = 2(\Phi_{mol} - \Phi_{Cu})$ along the molecular axis.

clean substrate, respectively. In this way, the variation of the work function across the molecular plane is independent from the work function of the tip.

To correlate these observations with the molecular structure, we modelled the interaction of a single PVBA molecule with the supporting metal by means of density functional theory calculations (see Methods). We find that in its stable configuration the molecule is adsorbed planar on the surface and is chemically bonded through its terminal oxygen and the nitrogen atoms, to Cu atoms of the first surface layer. Owing to the strong reactivity of the carboxyl group on adsorption on the Cu surfaces[22–24], the molecule is deprotonated (see also Supplementary Information). The potential-barrier profile will depend on the state of charge of the adsorbed molecule, which in turn depends on the interaction between the molecule and the substrate. Our calculations indicate that this induces a substantial rearrangement of the electron-density distribution on the molecule and in its proximity on the metal surface. This provides the most robust indicator of local modification of the surface dipole and of a modulation of the local potential barrier (see Supplementary Information). The electron-density rearrangement depicted in Fig. 2 shows the accumulation (red) and depletion (blue) regions on the adsorbed molecule system on two planes, orthogonal and parallel to the surface. The main observed features are (1) a modulation of the charge rearrangement on the molecular body with a partial electron accumulation on the molecule (Fig. 2a) and (2) a depletion from the surface regions immediately close to the molecular ends, more pronounced and laterally extended at the carboxyl end of the molecule (Fig. 2b).

The experimental observation of a higher potential barrier in the region directly above the (hetero-) aromatic groups surrounded by a lower rim region is naturally interpreted on the basis of this electron-density rearrangement. Namely, if at least part of its electronic charge is retained on deprotonation, the adsorbed molecule will be overall negatively charged, and an increase of the tunnelling barrier with respect to the bare Cu(111) surface will be expected. Our results reveal a net negative electric-dipole distribution aligned with the z axis and located on the aromatic-group region. Integration over this region gives an estimated total dipole of -0.47 D. This also enables estimation of the excess effective charge of the molecule as about $-0.1e$ (see Supplementary Information). The opposite charging effect is observed on the rim region (green in Fig. 1d), where the electron depletion determines a net positive dipole distribution, lowering the local potential barrier.

We note that the relative increase in the barrier observed in this work above the molecular aromatic structure may seem to be in contrast with the work-function decrease observed on adsorption of benzene on the same surface[16,19]. This is, however, not surprising given the different charge state and functional-group

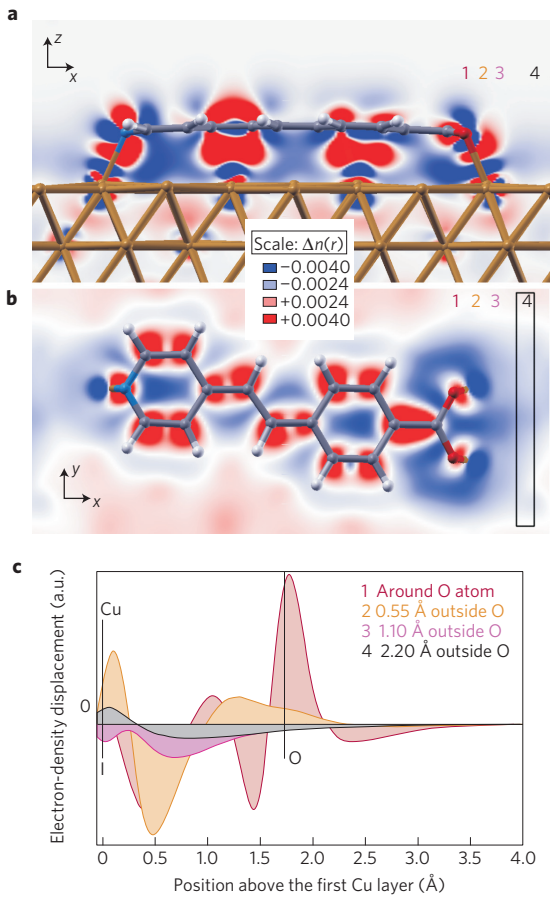

Figure 2 | Charge-transfer map of deprotonated PVBA absorbed on Cu(111). a, Side view (projection on a plane passing through the N–Cu and O–Cu bond). **b**, Top view (projection evaluated on a plane at halfway between the molecule and the surface). Blue areas represent electron depletion, red areas electron accumulation. The colour scale shows the variation of the local electron-density displacement in units of $Å^{-3}$. **c**, Averaged electron-density displacements along the *z* direction, calculated at different positions around the O–Cu bond, as indicated by the numbers in **a**. These are obtained by averaging the electron density in slices (0.5×7 $Å^2$) in the *xy* plane, as indicated in **b**. The vertical lines denote the positions of the atoms.

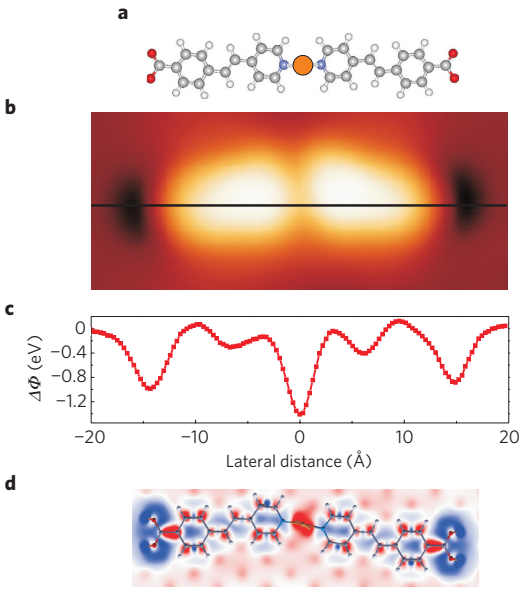

Figure 3 | Manipulation of the potential barrier by coordination bonding. a, Sketch of the metal–organic complex structure: two PVBA molecules are coordinated by a single Cu atom at the N terminations. **b**, STM topographic image of the coordination molecular complex on Cu(111). **c**, Variation of the work-function difference $\Delta\Phi$ measured along the molecular complex axis. **d**, Charge-transfer map of the coordination dimer.

structure of the deprotonated PVBA molecule characterized here. In the case of the neutral, non-reactive benzene molecule the observed decrease of the work function is mainly determined by the Pauli repulsion ('pillow effect'; refs 16, 19). In the present case, using the dipole value reported above and modelling the molecule as a flat capacitor as in ref. 25, the potential energy drop across the interface is estimated as 0.23 eV, in fair agreement with the work-function increase. The second key feature of the molecule–substrate interaction is the formation of an extended electron-depletion rim region surrounding the molecule. This is interpreted as a screening effect originating from the net negative charge distribution associated with the molecule. The depletion is more significant in the vicinity of the electronegative oxygen atoms bonded with the metal substrate. The lower potential barrier observed in front of the carboxyl group reflects the strong chemical interaction between the surface and this group, which is the principal anchoring point on the substrate for the adsorbed molecule. Taking the neutral deprotonated PVBA molecule and the bare surface as reference reactants, electrons from the metal region must be provided to form a σ-bond with the oxygen atoms. An area of charge depletion is clearly visible in the map of the electron-density displacement on the surface around the deprotonated carboxyl group (Fig. 2b).

The electron-density displacement $\Delta\rho$ as a function of the *z* coordinate, calculated for different positions along the molecular main axis (*x* direction), is reported in Fig. 2c. The largest modulations of the electron-density displacement are observed on the O and Cu atoms participating in the bonds (curves 1 and 2). However, purely negative displacement profiles indicating electron depletion are obtained in a region of the surface extending up to 2.5 Å from the carboxyl group (curves 3 and 4 in Fig. 2c). This effectively determines a positive vertical dipole density consistent with the lower local potential barrier experimentally measured in the rim region of Fig. 1. The effect is most pronounced in the area surrounding the Cu–O bond (curve 3 in Fig. 2c) in agreement with the barrier minimum position in Fig. 1d.

We note that simply assuming the oxygen atoms to be negatively charged would suggest a work-function increase on the oxygen atoms, because the lower electrostatic potential would make the tunnelling barrier on average higher in their proximity. Any such effect is, however, strongly reduced by the net polarization associated with bond formation. In particular, the electron density on the oxygen atoms moves towards the surface to form the Cu–O bond, showing that bond formation is associated with a positive electric dipole, screening the effect above (Fig. 2a).

Moreover, in standard topographic imaging 'tip-broadening' effects can enhance the apparent lateral extension of prominent surface features such as an adsorbed molecule, as these contribute a higher amount of the measured tunnelling current. If the tunnelling-current decay is instead measured, as we do here, the lower barrier rim region associated with a more slowly decaying current will be broadened instead, so that we expect a relative 'shrinkage', rather than a broadening, of the apparent molecular size in the potential-barrier map. The extent of this effect is revealed by comparing the extension of the constant-current signal (Fig. 1c) and the potential-barrier profile (Fig. 1d), showing that the latter technique yields a minimum located about 1.0 Å further inside the molecule than given by standard topographic imaging.

The capability to manipulate the built-in potential at the metal–molecule interface is of paramount importance for applications of organic molecules in any device entailing charge injection. To this end the extreme sensitivity to local charge rearrangements opens up new possibilities. This is documented in Fig. 3, where we demonstrate a dramatic local decrease of the work function (about 1.4 eV) by bonding a single copper atom to the pyridine end of two PVBA molecules. This structure is predicted as energetically favourable and is reminiscent of the coordination compounds observed for similar molecules[26]. Indeed, metal–organic coordination bonding has proven to be a very elegant and efficient strategy for the supramolecular nanostructuring of surfaces[26–28]. Additionally, this mimics the conventional procedure used in metal–organic devices. As the metal electrode is evaporated on top of the organic layer, metal ions interdiffuse and form covalent bonds with the molecular layer[3].

The drop of $\Delta\Phi$ at the oxygen-terminated side of the molecular complex resembles that observed for the single PVBA monomer adsorbed on Cu(111). However, a very significant decrease of the work function is now visible at the centre of the metal–organic complex, where the Cu adatom is located. The electron-density displacement map, shown in Fig. 3d, supports the experimental evidence. Furthermore, charge accumulation (red) and depletion areas (blue), not visible at the height position of this projection, indicate the presence of a positive induced dipole associated with electron-density transfer from the molecule through the bridging Cu atom. On the formation of a metal–organic bond at the N termination of PVBA, a charge reorganization occurs at the molecular backbone. This lowers substantially the effective electronic potential energy at the pyridine group with respect to the clean copper surface.

We believe that our findings relating the chemical bonding of PVBA to Cu(111) and the potential-barrier profile measured by STM may apply more generally to the formation of a potential barrier at the contact between an organic molecule and a metal electrode. In addition to illustrating these relations for a specific model system, our study reveals that the potential barrier can be monitored and manipulated in a controlled and defined way with atomic precision.

Methods

The experiments were carried out using a home-built scanning tunnelling microscope operated at 6 K in ultrahigh vacuum with a base pressure of 1×10^{-11} mbar. The Cu(111) single crystal has been cleaned in ultrahigh vacuum by cycles of Ar^+ ion sputtering and annealing. The PVBA molecules were deposited from a Knudsen cell at 450 K on a copper substrate held at 300 K.

The structural optimizations and the local-dipole calculations have been carried out with density functional theory methods within the plane-wave framework, by means of the Quantum-ESPRESSO package[29]. A computational (6×6) triclinic supercell with 16.71×16.71 Å^2 surface area was used, allowing 12 Å of vacuum between periodic images along the z axis (orthogonal to the surface) to avoid spurious interactions. The Cu(111) surface was modelled by means of a slab consisting of three metal layers with the coordinates of the deepest kept fixed to mimic the bulk arrangement. The adsorption was carried out on only one side of the slab, avoiding spurious dipole effects by means of the technique described in ref. 30. Vanderbilt ultrasoft pseudopotentials with a plane-wave kinetic-energy cutoff of 25 Ryd were used. Due to the large lateral cell dimensions, Brillouin zone sampling was limited to the Γ point. The convergence threshold for the residual forces during atomic-structure relaxation was set at 0.007 eV Å^{-1}; electronic exchange and correlation were treated within the local density approximation (LDA) approximation (Supplementary Information).

Received 11 August 2009; accepted 21 December 2009; published online 24 January 2010

References

1. Park, Y. D., Lim, J. A., Lee, H. S. & Cho, K. Interface engineering in organic transistors. *Mater. Today* **10,** 46–54 (2007).
2. Soubatch, S., Temirov, R. & Tautz, F. S. Fundamental interface properties in OFETs: Bonding, structure and function of molecular adsorbate layers on solid surfaces. *Phys. Status Solidi A* **205,** 511–525 (2008).
3. Friend, R. H. *et al.* Electroluminescence in conjugated polymers. *Nature* **397,** 121–128 (1999).
4. Janata, J. & Josowicz, M. Conducting polymers in electronic chemical sensors. *Nature Mater.* **2,** 19–24 (2002).
5. Nitzan, A. & Ratner, M. A. Electron transport in molecular wire junctions. *Science* **300,** 1384–1389 (2003).
6. Xu, B. & Tao, N. J. Measurement of single-molecule resistance by repeated formation of molecular junctions. *Science* **301,** 1221–1223 (2003).
7. Smit, R. H. M. *et al.* Measurement of the conductance of a hydrogen molecule. *Nature* **419,** 906–909 (2002).
8. Reed, M. A., Zhou, C., Muller, C. J., Burgin, T. P. & Tour, J. M. Conductance of a molecular junction. *Science* **278,** 252–254 (1997).
9. Ishii, H., Sugiyama, K., Ito, E. & Seki, K. Energy level alignment and interfacial electronic structures at organic/metal and organic/organic interfaces. *Adv. Mater.* **11,** 605–625 (1999).
10. Cahen, D. & Kahn, A. Electron energetics at surfaces and interfaces: Concept and experiments. *Adv. Mater.* **15,** 271–277 (2003).
11. Duhm, S. *et al.* Orientation-dependent ionization energies and interface dipoles in ordered molecular assemblies. *Nature Mater.* **7,** 326–332 (2008).
12. Seitsonen, A. P. *et al.* Density functional theory analysis of carboxylate-bridged diiron units in two-dimensional metal–organic grids. *J. Am. Chem. Soc.* **128,** 5634–5635 (2006).
13. Wandelt, K. *Thin Metal Films and Gas Chemisorption* 280 (Elsevier, 1987).
14. Bagus, P. S., Staemmler, V. & Wöll, C. Exchangelike effects for closed-shell adsorbates: Interface dipole and work function. *Phys. Rev. Lett.* **89,** 096104 (2002).
15. Leung, T. C., Kao, C. L., Su, W. S., Feng, Y. J. & Chan, C. T. Relationship between surface dipole, work function and charge transfer: Some exceptions to an established rule. *Phys. Rev. B* **68,** 195408 (2003).
16. Velic, D., Hotzel, A., Wolf, M. & Ertl, G. Electronic states of the C_6H_6/Cu(111) system: Energetics, femtosecond dynamics, and adsorption morphology. *J. Chem. Phys.* **109,** 9155–9165 (1998).
17. De Renzi, V. *et al.* Metal work-function changes induced by organic adsorbates: A combined experimental and theoretical study. *Phys. Rev. Lett.* **95,** 046804 (2005).
18. Ploigt, H.-C., Brun, C., Pivetta, M., Patthey, F. & Schneider, W.-D. Local work function changes determined by field emission resonances: NaCl/Ag(100). *Phys. Rev. B* **76,** 195404 (2007).
19. Dougherty, D. B., Maksymovych, P., Lee, J. & Yates, J. T. Jr Local spectroscopy of image-potential-derived states: From single molecules to monolayers of benzene on Cu(111). *Phys. Rev. Lett.* **97,** 236806 (2006).
20. Zerweck, U., Loppacher, C., Otto, T., Grafström, S. & Eng, L. M. Accuracy and resolution limits of Kelvin probe force microscopy. *Phys. Rev. B* **71,** 125424 (2005).
21. Olesen, L. *et al.* Apparent barrier height in scanning tunneling microscopy revisited. *Phys. Rev. Lett.* **76,** 1485 (1996).
22. Sotiropoulos, A., Milligan, P. K., Cowie, B. C. C. & Kadodwala, M. A structural study of formate on Cu(111). *Surf. Sci.* **444,** 52–60 (2000).
23. Johnston, S. M., Rousseau, G., Dhanak, V. & Kododwala, M. The structure of acetate and trifluoroacetate on Cu(111). *Surf. Sci.* **477,** 163–173 (2001).
24. Lin, N. *et al.* Two-dimensional adatom gas bestowing dynamic heterogeneity on surfaces. *Angew. Chem. Int. Ed.* **44,** 1488–1491 (2005).
25. Rusu, P.C., Giovannetti, G., Weijtens, C., Coehoorn, R. & Borcks, G. Work function pinning at metal–organic interfaces. *J. Phys. Chem. C* **113,** 9974–9977 (2009).
26. Tait, S. L. *et al.* One-dimensional self-assembled molecular chains on Cu(100): Interplay between surface-assisted coordination chemistry and substrate commensurability. *J. Phys. Chem. C* **111,** 10982–10987 (2007).
27. Barth, J. V., Costantini, G. & Kern, K. Engineering atomic and molecular nanostructures at surfaces. *Nature* **437,** 671–679 (2005).
28. Gambardella, P. *et al.* Supramolecular control of the magnetic anisotropy in two-dimensional high-spin Fe arrays at a metal interface. *Nature Mater.* **8,** 189–193 (2009).
29. Baroni, S. *et al.* <http://www.quantum-espresso.org>.
30. Bengtsson, L. Dipole correction for surface supercell calculations. *Phys. Rev. B* **59,** 12301 (1999).

Acknowledgements

We thank Mario Ruben for synthesizing the PVBA. A.D.V. and G.L. acknowledge funding from EPSRC grant EP/G044864/1 and the ESF-EUROCORES SONS Programme.

Author contributions

All authors contributed extensively to the work.

Additional information

The authors declare no competing financial interests. Supplementary information accompanies this paper on www.nature.com/naturematerials. Reprints and permissions information is available online at http://npg.nature.com/reprintsandpermissions. Correspondence and requests for materials should be addressed to L.V.